Strong localization effect in magnetic two-dimensional hole systems

U. Wurstbauer,[1,2,a)] S. Knott,[2] A. Zolotaryov,[2] D. Schuh,[1] W. Hansen,[2] and W. Wegscheider[1,3]

[1]*Institute of Experimental and Applied Physics, University of Regensburg, 93040 Regensburg, Germany*
[2]*Institute of Applied Physics, University of Hamburg, 20355 Hamburg, Germany*
[3]*Solid State Physics Laboratory, ETH Zurich, 8093 Zurich, Switzerland*

(Received 16 October 2009; accepted 20 December 2009; published online 12 January 2010)

We report an extensive study of the magnetotransport properties of magnetically doped two-dimensional hole systems. Inverted manganese modulation doped InAs quantum wells with localized manganese ions providing a magnetic moment of $S=5/2$ were grown by molecular beam epitaxy. Strong localization effect found in low-field magnetotransport measurements on these structures can either be modified by the manganese doping density or by tuning the two-dimensional hole density p via field effect. The data reveal that the ratio between p and manganese ions inside or in close vicinity to the channel enlarges the strong localization effect. Moreover, asymmetric broadening of the doping layer due to manganese segregation is significantly influenced by strain in the heterostructure. © *2010 American Institute of Physics*. [doi:10.1063/1.3291673]

Manganese (Mn) doped III-V,[1] II-VI,[2,3] and IV[4,5] semiconductor heterostructures are currently studied intensely because of their prospect for spin polarized charge carrier injection needed for spintronic applications. Low-dimensional InAs based heterostructures offer advantageous properties for spintronics such as large g-factor and spin-orbit interaction.[6,7] Moreover, Mn modulation-doped InAs-based heterostructures provide the possibility to study the interplay of localized magnetic moments of $S=5/2$ with spins of high-mobility hole systems.[8,9] Furthermore, modulation doping results in higher charge carrier mobilities compared to conventional diluted magnetic semiconductors (DMS) such as GaMnAs or InMnAs, which are only metallic for very high densities of magnetic impurities.[1] Huge negative magnetoresistance (NMR) associated with a magnetic-field induced insulator-to-metal transition, which are characteristic features of magnetic semiconductors,[2,3,5,10] were reported for inverted Mn modulation doped two-dimensional hole gases (2DHGs). Hysteretic behavior and abrupt resistance changes over several orders of magnitudes at subkelvin temperatures were also found in this material system.[9,11]

In this letter, we systematically investigate the influence of 2D hole density p, Mn doping concentration, strain, and quantum-well (QW) design on the MR behavior and the strong localization effect observed in inverted Mn modulation doped QW structures. The strong localization seems to be caused by Mn ions in the channel hosting the 2DHG. A significant amount of Mn ions is formed in inverted Mn doped heterostructures due to an asymmetric broadening of the doping layer as confirmed by secondary ion mass spectroscopy.[8] The Mn content in the QW is reported to be about 1% of the concentration in the doping layer, which is below 2×10^{20} cm^{-3}. We found similar localization effects indicated by NMR in a nonmagnetic carbon (C) modulation and additional Mn *co-doped* InAs QW structure demonstrating localization of 2D holes on Mn ions in close vicinity to be responsible for the peculiar low-field magnetotransport behavior.

In this study, the 2D hole density p is independently varied via field effect or Mn doping concentration. Therefore, modulation doped $In_{0.75}Al_{0.25}As/In_{0.75}Ga_{0.25}As/InAs$ QW structures were grown by molecular beam epitaxy on semi-insulating (001) GaAs substrates. Due to the large lattice mismatch between GaAs and $In_{0.75}Ga_{0.25}As$ metamorphic step graded buffers were used for strain relaxation. With these buffers the strain in the active layers can be tuned from compressive to tensile. For strain relaxation and strain variation in the active regions we follow the recipes given in Refs. 9 and 12 to get compressive and in Ref. 13 for tensile strain. Using a conventional buffer,[12] the In mole fraction was gradually increased from 0% to 75% in steps of 5% resulting in a residual compressive strain at the end of the metamorphic buffer. With an overshoot technique, the In mole fraction is increased with optimized steps for strain relaxation starting from 15% up to 80% and immediately reduced to 75% creating tensile strain in the layers grown afterwards.[13]

Crystal quality was tested and strain was determined by x-ray diffraction (XRD) investigations. The measurements were performed at the bending-magnet beam-line E2 of HASYLAB/DESY with a photon energy of 11.5 keV ($\lambda=0.107\,65$ nm) and with an instrumental angular resolution better than 0.005°. For electronic characterization, magnetotransport measurements were performed on 1 mm $\times 200$ μm Hall-bars aligned along the $[\bar{1}10]$ crystallographic direction at $T=4.2$ K with magnetic fields up to $B=14$ T using standard low-frequency lock-in technique with operation current of 100 nA. Ohmic contacts were prepared using annealed InZn. On some samples a 130 nm thin insulating parylene film followed by a metallic top-gate electrode consisting of 10 nm Ti and 120 nm Au was deposited.

The XRD measurements shown in Fig. 1 depict well-defined pattern originated from the active regions (marked with arrows) and demonstrate a good crystal quality in these layers. From $\Theta-2\Theta$ scans in the vicinity of the (004) GaAs Bragg reflection pattern shown in Fig. 1, the strain $\epsilon_\perp=\Delta a/a_0$ in the active regions was determined to $\epsilon_\perp=1.09$

a)Electronic addresses: uwurstba@physnet.uni-hamburg.de and ursula.wurstbauer@physnet.uni-hamburg.de.

 © 2010 American Institute of Physics

Downloaded 15 Sep 2010 to 131.169.95.144. Redistribution subject to AIP license or copyright; see http://apl.aip.org/about/rights_and_permissions

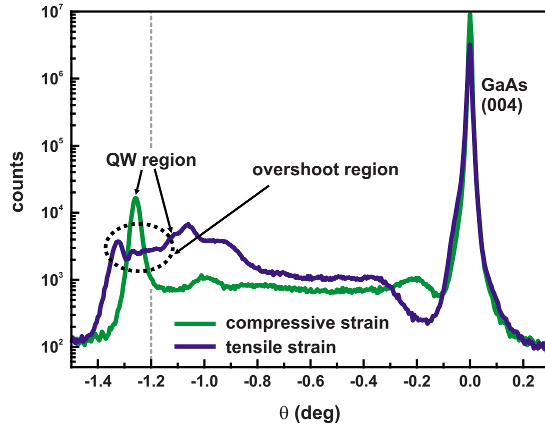

FIG. 1. (Color online) (004) X-ray diffraction curves for samples with conventional buffer and with overshoot. The arrows mark the peak arising from the active and the overshoot region according to the layer sequence. The dashed line denotes the diffraction angle expected for an unstrained $In_{0.75}Al_{0.25}As$ layer.

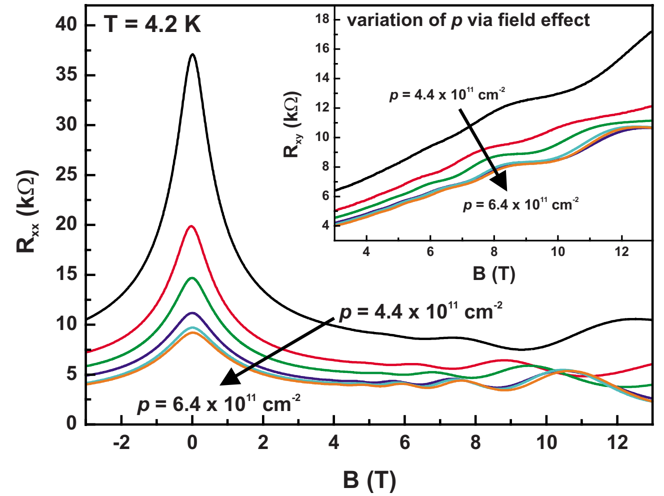

FIG. 2. (Color online) Longitudinal MR R_{xx} and Hall resistance traces R_{xy} (inset) at $T=4.2$ K in dependence of the 2D hole density p of one sample with a constant amount of Mn ions close to the 2DHG. The density was increased via field effect by applying a top-gate voltage (marked by arrows).

$\times 10^{-3}$ and -3.19×10^{-3} that points toward compressive and tensile strain, respectively. The strain in the metamorphic grown InAs channel was calculated using the measured lattice constant $a_{\perp}$ from the $In_{0.75}Ga_{0.25}As$ layer to $\epsilon_{\perp}=0.03$ for the conventional and $\epsilon_{\perp}=0.024$ for the overshoot buffer, respectively. In both cases the InAs channel hosting the 2DHG is compressively strained.

Now we focus on overall compressively strained QW structures grown on top of the conventional metamorphic buffer. The active region consists of a 7 nm thick InAlAs:Mn layer followed by an InAlAs spacer and a 20 nm InGaAs QW with an asymmetrically embedded 4 nm InAs channel and capped with 36 nm InAlAs. Width of the InAlAs spacer and the InGaAs QW as well as existence and position of the InAs channel was systematically modified. Therefrom we learned that the InAs channel is required to provide hole states above the Fermi-level E_F. Without the InAs channel a deep state is formed that cannot be ionized. The overall distance between doping layer and InAs channel is limited to about 10 nm to form a 2DHG. Both, InAlAs spacer and a part of the InGaAs QW serve as virtual spacer that constitute 7.5 nm for all samples discussed below. A scheme of the active layer sequence is inserted in Fig. 3(d). As depicted in Fig. 2, a large NMR and Shubnikov–de Haas (SdH) oscillations are developed in the longitudinal MR R_{xx} at $T=4.2$ K. A positive Hall coefficient and well-pronounced Hall plateaus are observable in the Hall resistance traces (inset in Fig. 2) demonstrating transport in a 2D hole system. The MR traces shown in Fig. 2 were measured with different top-gate voltages. It is clearly visible that the NMR and simultaneously the zero-field sheet resistivity $R_{xx}(0)$ decreases with increasing 2D carrier density. The 2D hole density p was determined from the $1/B$-periodicity of the SdH oscillations and confirmed by the slope of the Hall resistance R_{xy}.

To clarify the dependence of localization effects from the carrier density p, we investigate a couple of compressively strained QWs with different doping concentrations (effusion cell temperatures from 790 to 842 °C). Since the determination of such low Mn fluxes needed for low doping densities is rather imprecise, all samples were grown in a short period of time and the Mn flux variation is specified by the temperature of the Mn effusion cell. The carrier density of these samples ranges from $p=4.4\times 10^{11}$ cm^{-2} to 11.8×10^{11} cm^{-2}. The MR traces depicted in Fig. 3(a) demonstrate a clear trend that higher doping densities lead to higher hole densities and enhanced zero-field sheet resistivity. We found the existence of an upper limit of the Mn doping concentration from which the samples get insulating in the whole magnetic field range. In Fig. 3(b) the MR traces at 4.2 K are taken in dependence of the 2D carrier density p varied by field effect for one sample with a fixed amount of Mn ions in close proximity to the itinerant 2D holes. The carrier density was altered between $p=4.4\times 10^{11}$ cm^{-2} and 6.4×10^{11} cm^{-2} resulting in a modification of the zero-field sheet resistivity between 37.1 k$\Omega \geq R_{xx}(0) \geq 9.7$ kΩ. Here the trend is the other way round. Decreasing p increases the sheet resistivity $R_{xx}(0)$ and leads to stronger localization effects. Further depletion of the 2DHG still increases the sheet resistivity but the hole density p is not longer determinable with required accuracy. The findings are summarized in Fig. 3(d), where the zero sheet resistivity $R_{xx}(0)$ is plotted versus 2D hole density p for various Mn concentrations (triangles) taken from Fig. 3(a), for fixed Mn concentration (dots) from Fig. 3(b), and for two identically doped QWs with compressive and tensile strain at the end of the buffer (squares) ascertained from Fig. 3(c). Consequently, not only the carrier density p seems to affect the localization effect. Higher doping densities of the InAlAs:Mn layer results in an enhanced Mn segregation and thus in a higher amount of Mn in the InAs channel hosting the 2DHG and, therefore, in a lower ratio between free holes p and Mn. On the other hand, increasing the carrier density p by field-effect at a fixed amount of Mn in the channel increases the ratio between p and Mn. We infer that the zero-field sheet resistivity and therefore the localization effect is reduced by increasing the ratio between free holes p and Mn. Moreover, carrier density p and zero field sheet resistivity $R_{xx}(0)$ are both considerably enhanced from $p=10.8\times 10^{11}$ cm^{-2} and $R_{xx}(0)=43.3$ kΩ for compressive strain in the active region compared to $p=14.5\times 10^{11}$ cm^{-2} and $R_{xx}(0)=73.4$ kΩ for tensile strain. The quantum well structure in both samples consists of identical layer sequence and Mn doping density. We explain this finding by a changed profile of the asymmetric broadening of

Downloaded 15 Sep 2010 to 131.169.95.144. Redistribution subject to AIP license or copyright; see http://apl.aip.org/about/rights_and_permissions

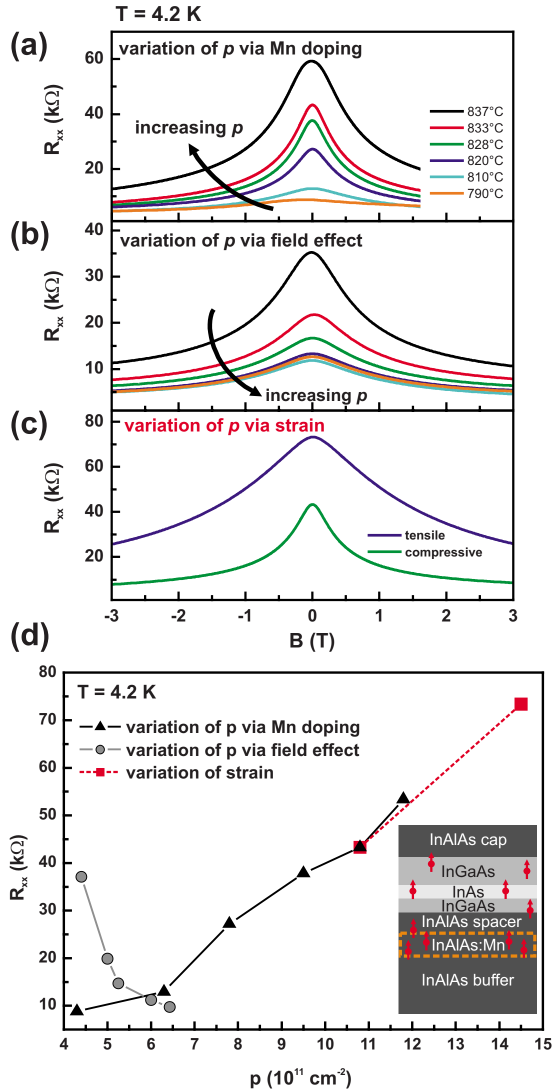

FIG. 3. (Color online) Longitudinal MR $R_{xx}(B)$ at $T=4.2$ K in dependence of Mn doping concentration (a) and field effect (b). (c) $R_{xx}(B)$ at $T=4.2$ K for tensile and compressive strained active layers modulation doped with identical Mn concentrations in the doping layer. (d) Zero field resistance $R_{xx}(0)$ taken from (a) (triangles), (b) (dots), and (c) (squares) as a function of the 2D carrier density p.

the doping layer. The Mn segregation is dramatically enlarged for tensile strain and therefore the 2D hole density p is increased. Consequently, the ratio between p and Mn in the InAs channel is reduced and thus the localization effect enhanced.

To sum up, we have demonstrated that the strong localization effect in magnetic Mn *co-doped* 2DHGs confined in InAs QWs depends on the ratio between itinerant holes p and Mn in the 2D channel. The ratio can be tuned indirectly by Mn doping density because of the asymmetric broadening of the doping layer due to segregation and directly by varying the 2D hole density p for a fixed amount of Mn via field effect. Changing the strain from compressive to tensile strain affects the Mn segregation and hence the ratio of p and Mn inside the channel and consequently the localization effect.

Concluding from our results, inverted Mn modulation doped InAs QW structures faciliate the fabrication of strongly DMSs with proper charge carrier mobility, which is not possible with most of the conventional DMS materials. Because both, Mn concentration and hole density in the QW, are adjustable independently from each other, this material system provides the possibility to fabricate highly tunable laterally defined magnetic and semiconducting nanostructures. For instance, diluted magnetic quantum dots (DMQDs) made from this material system might have advantageous properties such as precisely tunable size, density of Mn impurities and charge carriers in contrast to self-organized strain induced InAs DMQDs.[14] Such structures might be suitable to enable the investigation of, e.g., RKKY interaction in low dimensions or Kondo effect in the presence of magnetic impurities[15] in DMS materials.

We acknowledge financial support by the DFG via Program Nos. SFB 508 and SFB 689 and by the cluster of Excellence *Nanospintronics*.

[1] T. Dietl, H. Ohno, F. Matsukura, J. Cibert, and D. Ferrand, Science **287**, 1019 (2000).
[2] P. Smorchkova, N. Samarth, J. Kikkawa, and D. D. Awschalom, Phys. Rev. Lett. **78**, 3571 (1997).
[3] J. Jaroszyński, T. Andrearczyk, G. Karczewski, J. Wrobel, T. Wojtowicz, D. Popovic, and T. Dietl, Phys. Rev. B **76**, 045322 (2007).
[4] D. Bougeard, S. Ahlers, A. Trampert, N. Sircar, and G. Abstreiter, Phys. Rev. Lett. **97**, 237202 (2006).
[5] M. Jamet, A. Barski, T. Devillers, V. Poydenot, R. Dujardin, P. Bayle-Guillemaud, J. Rothman, E. Bellet-Amalric, A. Marty, J. Cibert, R. Mattana, and S. Tatarenko, Nature Mater. **5**, 653 (2006).
[6] D. Grundler, Phys. Rev. Lett. **84**, 6074 (2000).
[7] W. Desrat, F. Giazotto, V. Pellegrini, M. Governale, F. Beltram, F. Capotondi, G. Biasiol, and L. Sorba, Phys. Rev. B **71**, 153314 (2005).
[8] U. Wurstbauer and W. Wegscheider, Phys. Rev. B **79**, 155444 (2009).
[9] U. Wurstbauer, M. Soda, R. Jakiela, D. Schuh, D. Weiss, J. Zweck, and W. Wegscheider, J. Cryst. Growth **311**, 2160 (2009).
[10] A. Oiwa, S. Katsumoto, A. Endo, M. Hirasawa, M. Iye, H. Ohno, H. Marsukura, F. Shen, and Y. Sugawara, Phys. Status Solidi B **205**, 167 (1998).
[11] U. Wurstbauer, I. Gronwald, U. Stöberl, A. Vogl, D. Schuh, D. Weiss, and W. Wegscheider, Physica E (Amsterdam) **40**, 1563 (2008).
[12] C. Heyn, S. Mendach, S. Löhr, S. Schnüll, and W. Hansen, J. Cryst. Growth **251**, 832 (2003).
[13] F. Capotondi, G. Biasiol, D. Ercolani, V. Grilla, E. Carlino, F. Romanato, and L. Sorba, Thin Solid Films **484**, 400 (2005).
[14] M. Holub, S. Chakrabarti, S. Fathpour, P. Bhattacharya, Y. Lei, and S. Ghosh, Appl. Phys. Lett. **85**, 973 (2004).
[15] H. B. Heersche, Z. de Groot, J. A. Folk, L. P. Kouwenhoven, and H. S. J. van der Zant, Phys. Rev. Lett. **96**, 017205 (2006).

Downloaded 15 Sep 2010 to 131.169.95.144. Redistribution subject to AIP license or copyright; see http://apl.aip.org/about/rights_and_permissions